IV International Conference on Particle-based Methods – Fundamentals and Applications
PARTICLES 2015
E. Oñate, M. Bischoff, D.R.J. Owen, P. Wriggers & T. Zohdi (Eds)

DEVELOPMENT OF HIGHER ORDER PARTICLE DISCRETIZATION SCHEME FOR ANALYSIS OF FAILURE PHENOMENA

Mahendra Kumar Pal[1], Maddegedara L.L. Wijerathne[2], Muneo Hori[2], Tsuyoshi Ichimura[2] and Seizo Tanaka[2]

[1] Department of Civil Engineering, The University of Tokyo
7-3-1 Hongo, Bunkyo-ku, Tokyo 113-8656 Japan
e-mail: mahendra@eri.u-tokyo.ac.jp

[2] Earthquake Research Institute, The University of Tokyo
1-1-1 Yayoi, Bunkyo-ku, Tokyo, 113-0032, Japan
e-mails: lalith@eri.u-tokyo.ac.jp, hori@eri.u-tokyo.ac.jp, ichimura@eri.u-tokyo.ac.jp, tanaka.seizo@gmail.com

Key words: Higher order PDS, PDS-FEM, Local polynomial expansion, Conjugate tessellation, Mode-I crack

Abstract. This paper presents the higher order extension of Particle Discretization Scheme (PDS) and its implementation in FEM framework (PDS-FEM) to solve boundary value problems of linear elastic solids, including brittle cracks. Higher order PDS defines an approximation $f^d(\mathbf{x})$ of a function $f(\mathbf{x})$, defined over domain Ω, as the union of local polynomial approximation of $f(\mathbf{x})$ over each Voronoi tessellation elements of Ω. The support of the local polynomial bases being confined to the domain of each Voronoi element, $f^d(\mathbf{x})$ consists of discontinuities along each Voronoi boundaries. Considering local polynomial approximations over elements of Delaunay tessellation, PDS define bounded derivatives for this discontinuous $f^d(\mathbf{x})$. Utilizing the inherent discontinuities in $f^d(\mathbf{x})$, PDS-FEM proposes a numerically efficient treatment for modeling cracks. This novel use of local polynomial approximations in FEM is verified with a set of linear elastic problems, including mode-I crack tip stress field.

1 INTRODUCTION

Particle based numerical methods have been very popular and widely accepted in solid mechanics and computational fluid mechanics. A salient feature of particle methods is that they provide relatively simple treatments for modeling crack propagation, which is one area particle methods are widely used. The movements of crack tip singularity is highly sensitive to even the minor heterogenities in materials, external loading, etc., and

makes the crack path to produce wide range of behaviours like branching, bending, etc. Hence, it is essential to perform probabilistic analysis of crack-path variability, based on methods like statistical model[1] or Monte-Carlo simulation[2]. Construction of probability density function (PDF) of crack paths for a given problem requires a large number of simulations, skyrocketing the required computational resources. Hence, numerical methods with efficient failure treatments are necessary for realizing the need of constructing crack path PDF for practical applications.

Particle based numerical tool such as smooth particle method (SPH)[3], element free Galerkin method (EFGM)[4], reproducing kernel particle method (RKPM)[5] are efficient methods for failure analysis. Accuracy of these methods is improved by introducing some additional nodes in domain, where more refinement (*h-adaptivity*) is needed. However, these methods are not capable of incorporating the Poison's effect and encounter problems in enforcing the essential boundary conditions. While FEM has well established mathematical foundation, it is not numerically efficient in modeling crack propagation; requires complex treatments like introduction of new nodes, adaptive mesh refinements, etc. Recent advancement such as element free Galerkin method (EFGM)[4], partition of unity method (POU)[6], eXtended finite element method and other mesh-less methods enable accurate modeling of crack tip stress singularity, which is a function of $\sqrt{r}$, θ; (r, θ) is a polar coordinate system at the crack tip. In-spite of higher accuracy, these enhancements are complex to implement and introduce a hefty computational overhead. In nutshell, particle methods and finite element method have their own positive and negative features.

Considering the merits of finite element methods and particle methods, Particle Discretization Scheme (PDS) had been proposed[7, 8], and implemented into FEM framework (PDS-FEM). We refer this original work as 0^{th}-order PDS. PDS-FEM provides a numerically efficient failure treatment which allows one to construct PDF of 3D crack paths in large scale problems. This paper presents the higher order extension of PDS and PDS-FEM to simulate brittle elastic cracks. Just as in 0^{th}-order PDS, the higher order extension also uses the tessellations pair Voronoi and Delaunay, of a domain Ω, to approximate functions and their derivatives defined over Ω. Higher order PDS extension defines an approximation $f^d(\mathbf{x})$ of a function $f(\mathbf{x})$, defined over Ω, as the union of local polynomial approximation of $f(\mathbf{x})$ over each Voronoi tessellation elements. The support of the local polynomial bases being confined to the domain of each Voronoi element, $f^d(\mathbf{x})$ consists of discontinuities along each Voronoi boundaries. Considering local polynomial approximations over elements of Delaunay tessellation, PDS define bounded derivatives for this discontinuous $f^d(\mathbf{x})$. Further, exploiting the inherent discontinuities in $f(\mathbf{x})$ PDS-FEM propose a numerically efficient treatment for modeling cracks. This paper presents the higher order extension PDS-FEM and its numerically efficient treatment for modeling brittle elastic cracks. Some benchmark problems, including a mode-I crack tip problem, are presented to verify the higher order PDS-FEM.

This paper is consist of four other sections along with introduction. The second section

emphasis on the concept of higher order PDS. Implementation of PDS into finite element framework has been explained in third section. Numerical examples with the results are discussed in fourth section. Final section includes the concluding remark.

2 HIGHER ORDER PDS

A unique feature of PDS is the use of conjugate tessellations to approximate functions and their derivatives. In this paper, we use Voronoi and Delaunay tessellations pair for approximating functions and derivatives, respectively [7, 8]. PDS is not inherently bound to the tessellation pair Voronoi and Delaunay, and should work with any other conjugate domain tessellation pair.

Let $f(\mathbf{x})$ be a target function in an analysis domain V; Voronoi and Delaunay tessellations for V be $\{\Phi^\alpha\}$ and $\{\Psi^\beta\}$; $\mathbf{y}^\alpha$ and $\mathbf{z}^\beta$ be the mother points of Φ^α and the center of gravity of Ψ^β, respectively. Denoted by $\phi^\alpha(\mathbf{x})$ and $\psi^\beta(\mathbf{x})$ are the characteristic functions of Φ^α and Ψ^β, respectively. Here, the characteristics function of $\{\Phi^\alpha\}$ is defined such that $\phi^\alpha(\mathbf{x}) = 1$ if $\mathbf{x} \in \Omega^\alpha$ and $\phi^\alpha(\mathbf{x}) = 0$ if $\mathbf{x} \notin \Omega^\alpha$; $\psi^\alpha(\mathbf{x})$ follows similar definition.

Higher order PDS approximates a function $f(\mathbf{x})$ and its derivatives $f(\mathbf{x})_{,i}$ as

$$f(\mathbf{x}) \approx f^d(x) = \sum_{\alpha=1}^{N^\alpha} \sum_{n=0}^{|P^\alpha|} f^{\alpha n} P^{\alpha n}, \tag{1}$$

$$f(\mathbf{x})_{,i} \approx g_i^d(x) = \sum_{\beta=1}^{N^\beta} \sum_{m=0}^{|Q^\beta|} g_i^{\beta m} Q^{\beta m}, \tag{2}$$

where, $P^{\alpha n}(\mathbf{x}-\mathbf{y}^\alpha) \in P^\alpha = \{1, (\mathbf{x}-\mathbf{y}^\alpha), \ldots, (\mathbf{x}-\mathbf{y}^\alpha)^r, \ldots\}\,\phi^\alpha(\mathbf{x})$ and $Q^{\beta m}(\mathbf{x}-\mathbf{z}^\beta) \in Q^\beta = \left\{1, \left(\mathbf{x}-\mathbf{z}^\beta\right), \ldots, \left(\mathbf{x}-\mathbf{z}^\beta\right)^r, \ldots\right\}\psi^\beta(\mathbf{x})$. N^α is a number of Voronoi elements and N^β is a number of Delaunay elements.

The coefficients $f^{\alpha n}$'s and $g_i^{\beta n}$'s are found by minimizing the errors $E^f = \int (f(\mathbf{x}) - f^d(\mathbf{x}))^2 \,\mathrm{d}v$ and $E^g = \int \left\|\mathbf{g}^d(\mathbf{x}) - \nabla f^d(\mathbf{x})\right\|^2 \,\mathrm{d}v$, respectively. $\|.\|$ is the norm of a vector $(.)$. Minimization of E^f and E^g produce following pair of linear sets of equations, each of which can be solved to find $f^{\alpha m}$'s and $g_i^{\beta m}$'s

$$\sum_{m}^{|P^\alpha|} I^{\alpha nm} f^{\alpha m} = \int_{\Phi^\alpha} f(\mathbf{x}) P^{\alpha n}(\mathbf{x}-\mathbf{y}^\alpha)\,\mathrm{d}v \tag{3}$$

$$\sum_{m}^{|Q^\beta|} A^{\beta nm} g_i^{\beta m} = \sum_{\alpha,l} f^{\alpha l} \int_{\Psi^\beta} Q^{\beta n} \left(P^{\alpha l}(\mathbf{x}-\mathbf{z}^\beta)\right)_{,i}\,\mathrm{d}v. \tag{4}$$

$I^{\alpha nm}$ and $A^{\beta nm}$ are defined as $I^{\alpha nm} = \int_{\Phi^\alpha} P^{\alpha n} P^{\alpha m}\,\mathrm{d}v$ and $A^{\beta nm} = \int_{\Psi^\beta} Q^{\beta n} Q^{\beta m}\,\mathrm{d}v$. According to above formulations, it is straightforward to include the higher order polynomials

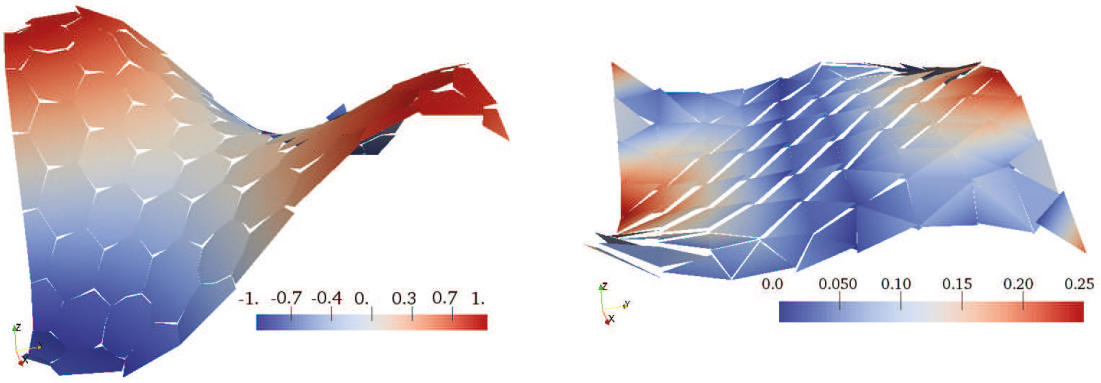

(a) $f(x,y) = \sin(^{xy}/_{40})$ (b) $^{\partial f(x,y)}/_{\partial x}$

Figure 1: $f(x,y) = \sin(^{xy}/_{40})$ and $^{\partial f(x,y)}/_{\partial x}$ approximated with higher order PDS; $P^\alpha = \{1,(x-x^\alpha),(y-y^\alpha)\}\phi^\alpha(\mathbf{x})$ and $Q^\beta = \{1,(x-x^\beta),(y-y^\beta)\}\psi^\beta(\mathbf{x})$.

in the original PDS[7, 8] that uses the characteristic functions as the basis functions of discretization.

As seen in Fig. 1(a), an approximation of a function obtained with higher order PDS contains discontinuities along the boundaries of Φ^α (i.e. $\partial\Phi^\alpha$'s). Hence PDS gets its particle nature. Nevertheless of the discontinuities, PDS defines bounded derivatives, smoothly connecting the discontinuous function approximation over the conjugate tessellation Ψ^β (see Fig. 1(b)). This allows one to use PDS in solving boundary value problems. As shown in the latter half of the next section, the discontinuities in $f^d(\mathbf{x})$ also contribute to derivative $g_i^d(x)$, which is conveniently exploited to implement an efficient treatment for modeling cracks in solids.

Numerical experiments show that the error of approximation diminish at a second order rate for both the function and derivatives as discussed in previous work [9]. Further, higher accuracy and convergence rates can be obtained by including higher order polynomials to the sets P^α and Q^β.

3 HIGHER ORDER PDS-FEM

3.1 Formulation

Consider standard Boundary Value Problem (BVP) of infinitesimal deformation of a linearly elastic body occupying the space V. We ignore body forces for the sake of simplicity. This section presents the implementation of higher order PDS in FEM framework to solve this BVP. We us the following standard Lagrangian as the weak form for this BVP.

$$\mathcal{L}(\boldsymbol{\epsilon},\mathbf{c}) = \frac{1}{2}\int \boldsymbol{\epsilon} : \mathbf{c} : \boldsymbol{\epsilon}\, \mathrm{d}v \tag{5}$$

We approximate the displacement field $\mathbf{u}$ and $\nabla\mathbf{u}$ as

$$u_i \approx \sum_{\alpha} u_i^{\alpha} = \sum_{\alpha} \sum_{m}^{|P^{\alpha}|} u_i^{\alpha m} P^{\alpha m} \tag{6}$$

$$u_{i,j} \approx \sum_{\beta} g_{ij}^{\beta} = \sum_{\beta} \sum_{n}^{|Q^{\beta}|} g_{ij}^{\beta n} Q^{\beta n} \tag{7}$$

The unknown $g_{ij}^{\beta n}$'s can be found by minimizing the error $E^{\mathbf{g}} = \sum_{\beta} \int_{\Psi^{\beta}} \left\| g_{ij}^{\beta} \mathbf{e}_i \otimes \mathbf{e}_j - \nabla \mathbf{u}^{\alpha} \right\|^2 \mathrm{d}v$ with respect to $g_{ij}^{\beta n}$.

$$g_{ij}^{\beta n} = \left(B^{\beta n n'} \int_{\Psi^{\beta}} Q^{\beta n'} \left(P^{\alpha m} \right)_{,j} \mathrm{d}v \right) u_i^{\alpha m} \tag{8}$$

$$= b_j^{\beta n \alpha m} u_i^{\alpha m}. \tag{9}$$

where $\left[B^{\beta n n'} \right] = \left[A^{\beta n' n} \right]^{-1}$. For the sake of brevity, the above tensor equations can be expressed as

$$\mathbf{g}^{\beta n} = \mathbf{b}^{\beta n \alpha m} \otimes \mathbf{u}^{\alpha m} \tag{10}$$

With Eq. 10, and approximation scheme of PDS, strain: $\boldsymbol{\epsilon}$ can be approximated as $\boldsymbol{\epsilon} \approx \sum_{\beta,n} \boldsymbol{\epsilon}^{\beta n} Q^{\beta n}$, where

$$\boldsymbol{\epsilon}^{\beta n} = sym \left(\mathbf{b}^{\beta n \alpha m} \otimes \mathbf{u}^{\alpha m} \right) \tag{11}$$

and *sym* stands for symmetric part of the second order tensor. Further, $\boldsymbol{\sigma}$ is determined as $\boldsymbol{\sigma}^{\beta} = \mathbf{c}^{\beta} : \boldsymbol{\epsilon}^{\beta}$, where $\mathbf{c}^{\beta}$ is the constitutive tensor for Ψ^{β}.

With the above definitions, implementation of PDS in FEM framework is straightforward. Substituting Eq. 11 into Eq. 5 and setting its first variation $\delta\mathcal{L} = 0$, following linear set of equations can be obtained

$$\sum_{\alpha' m'} \sum_{n,n'} A^{\beta n n'} \left(\mathbf{b}^{\beta n \alpha m} . \mathbf{c} . \mathbf{b}^{\beta n' \alpha' m'} \right) . \mathbf{u}^{\alpha' m'} = \mathbf{0}.$$

In the above set of governing equations, the stiffness matrix for a Delaunay tessellation Ψ^{β} can be readily recognized as

$$\mathbf{k}^{\beta} = \sum_{n,n'} A^{\beta n n'} \left(\mathbf{b}^{\beta n \alpha m} . \mathbf{c} . \mathbf{b}^{\beta n' \alpha' m'} \right),$$

where $\mathbf{k}^{\beta}$ is a matrix of size $(6\,|P^{\alpha}|) \times (6\,|P^{\alpha}|)$ or $(12\,|P^{\alpha}|) \times (12\,|P^{\alpha}|)$ with triangular element in 2D or tetrahedral elements in 3D, respectively.

3.2 Modeling brittle fracture with PDS-FEM

As mentioned, a major advantage of PDS-FEM is the simple and numerically efficient treatment for modelling discontinuities. PDS approximation $f^d(\mathbf{x})$ of a function $f(\mathbf{x})$ inherently consists of discontinuities along each edge of Voronoi elements $\partial\Phi^\alpha$'s, which are clearly visible in Fig. 1(a). When PDS defines bounded derivatives for $f^d(\mathbf{x})$ over Ψ^β, contribution from these discontinuities along $\partial\Phi^\alpha$'s are also taken in to account (Eq. 4). In PDS-FEM, a brittle crack along a segment of a given $\partial\Phi^\alpha$ is modeled by dropping those contributions from an infinitesimal neighbourhood of the relevant $\partial\Phi^\alpha$. As explained below, this failure treatment requires nothing more than recalculation of a single element stiffness matrix.

According to the definition, $P^{\alpha n}$ can be written as $P^{\alpha n} = F^{\alpha n}\left(\mathbf{x}-\mathbf{y}^\alpha\right)\,\phi^\alpha(\mathbf{x})$, which allows to express $b_j^{\beta n\alpha m}$ in Eq. 9 as

$$b_j^{\beta n\alpha m} = \sum_{n'}^{|Q^\beta|} B^{\beta nn'} \int_{\Psi^\beta} Q^{\beta n'}\left(F^{\alpha m}_{,j}\,\phi^\alpha + F^{\alpha m}\phi^{\alpha}_{,j}\right)\mathrm{d}v \tag{12}$$

$$= \sum_{n'}^{|Q^\beta|} B^{\beta nn'}\left(\int_{\Psi^\beta} Q^{\beta n'} F^{\alpha m}_{,j}\,\phi^\alpha\,\mathrm{d}v + \int_{\partial\Phi^\alpha} Q^{\beta n'} F^{\alpha m} n_j\,\mathrm{d}s\right), \tag{13}$$

where, n_j^α is the unit outward normal along $\partial\Phi^\alpha$. In Eq. 13, the term $\int_{\partial\Phi^\alpha} Q^{\beta n'} F^{\alpha m} n_j\,\mathrm{d}s$ is responsible for including the contribution to ϵ_{ij}^β from the discontinuities along $\partial\Phi^\alpha$ in the approximated displacement field.

What is required to model a brittle crack along a segment of Voronoi boundary, $\partial\Phi^\alpha$, is dropping this contribution $\int_{\partial\Phi^\alpha} Q^{\beta n'} F^{\alpha m} n_j\,\mathrm{d}s$ from the corresponding segment of $\partial\Phi^\alpha$, when evaluating $\mathbf{b}^{\beta n\alpha m}$. As an example, to model a crack along the boundary AG creating a crack surfaces AG and GA′ in Fig. 2(b), all it needs is to exclude the contributions $\int_{AG} Q^{\beta n'} F^{\alpha_1 m} n_j^{\mathrm{AG}}\,\mathrm{d}l$ and $\int_{\mathrm{A'G}} Q^{\beta n'} F^{\alpha_2 m} n_j^{\mathrm{A'G}}\,\mathrm{d}l$, when evaluating $\mathbf{b}^{\beta n\alpha m}$, and recalculate the element stiffness matrix of corresponding Delaunay element. The integration $\int_{\partial\Phi^\alpha} Q^{\beta n'} F^{\alpha m} n_j\,\mathrm{d}s$ can easily be evaluated with numerical integration over lines/planes in 2D/3D settings, respectively.

Compared with the treatments used in other methods to model propagating cracks, this treatment is simple and numerically efficient. Most existing numerical methods which requires introduction of new nodes, enrichment involving complex integration and introduction of new DOFs, etc., while above PDS-FEM treatment require only recalculation of an element stiffness matrix. Especially, in simulating large scale problems utilizing high performance computing, this simple crack treatment has a clear advantage over the existing methods.

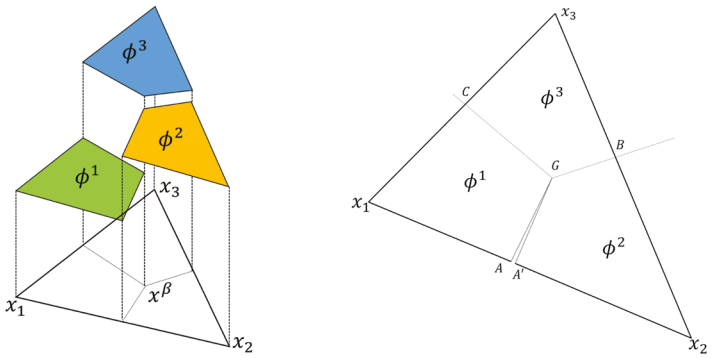

Figure 2: Simulation of crack; (a) existing discontinuities in the displacement field approximated with PDS, (b) modeling a crack by dropping contribution from infiniticimally thin neighborhood of the Vorono boundary to be broken.

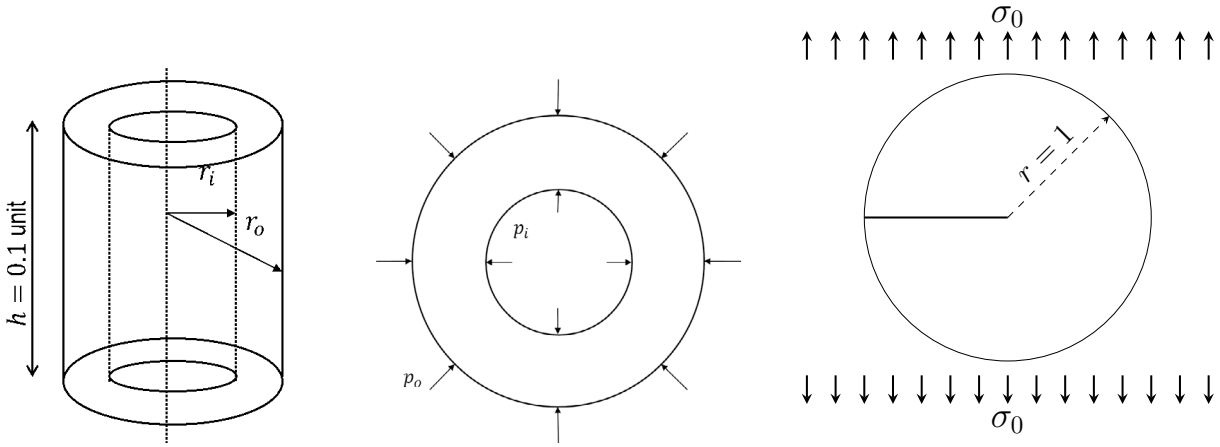

(a) cylinder geometry (b) $p_i = 50$MPa, $p_0 = 100$MPa (c) mode-I edge crack problem

Figure 3: Settings of the thick cylinder and mode-I edge crack problems.

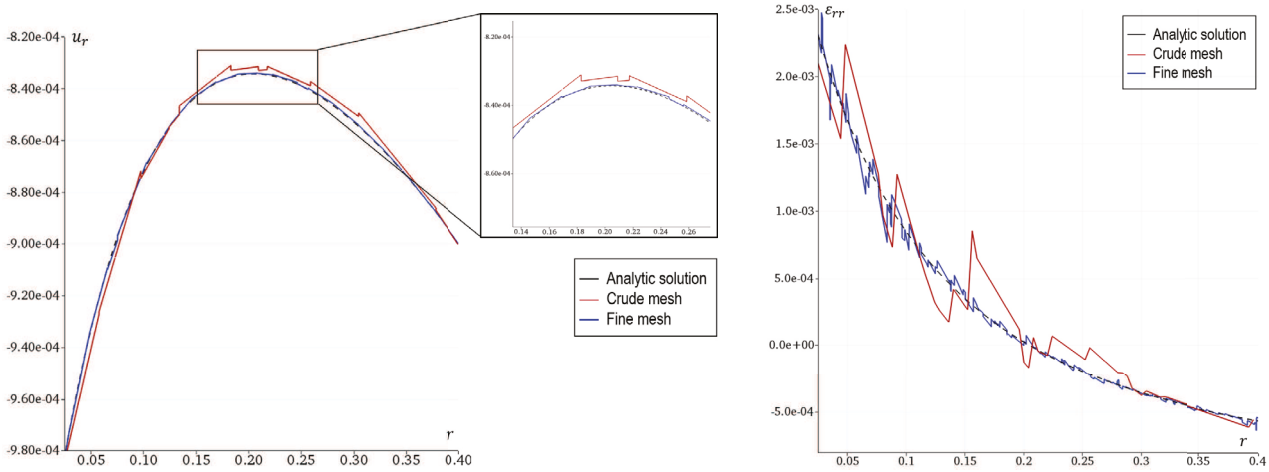

(a) (b)

Figure 4: (a) Displacement: u_r and (b) strain: ϵ_{rr} along radial direction

4 NUMERICAL EXAMPLES

In this section, we present some numerical results to verify the of higher order extension of PDS-FEM. Specifically, the analytic solutions and numerical results are compared for the problem of thick cylinder subjected internal and external pressure, and mode-I crack subjected to far field loading.

4.1 Thick cylinder under internal and external pressure

A thick cylinder subjected to internal and external pressure, which is a classical problem, is considered to verify the 3D implementation of PDS-FEM. The problem settings are illustrated in Fig. 3(a) and (b). The boundary conditions at the cylinder ends are set to reproduce plain strain conditions. The set of polynomial bases used are

$$
\begin{aligned}
P^\alpha &= \{1, (x-x^\alpha), (y-y^\alpha), (z-z^\alpha)\} \\
Q^\beta &= \{1, (x-x^\beta), (y-y^\beta), (z-z^\beta), (x-x^\beta)^2, (y-y^\beta)^2, (z-z^\beta)^2, (x-x^\beta)(y-y^\beta), \\
&\quad (x-x^\beta)(z-z^\beta), (y-y^\beta)(z-z^\beta)\}
\end{aligned}
$$

Figure 4 compares the analytic solutions and numerical results of radial displacement u_r and strain component ϵ_{rr}, along a radial line. A quick comparison advocates the improvement in solution with the mesh refinement, and that the numerical solutions are in good agreement with analytic solution. For this specific setting, u_r reaches its maximum at $r = 0.2$. Figure 5 shows the error of u_r and ϵ_{rr} at $r = 0.2$, for several tessellations with different element sizes. As is seen, the error diminishes at a second order rate with respect to the number of degrees of freedoms, which is the expected.

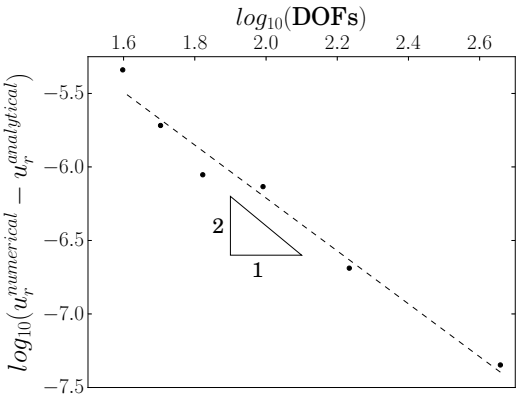

Figure 5: Error in u_r at $r = 0.4$ for the thick cylinder problem with 1^{st}-order PDS-FEM; obtained with tessellations of different element sizes.

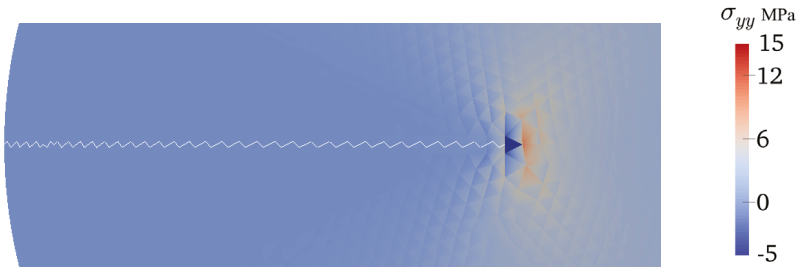

Figure 6: σ_{yy} in the crack tip neighborhood. White lines are broken Voronoi boundaries.

4.2 Stress singularity at a mode-I crack tip

In order to verify the crack treatment proposed in section 3.2, the classical 2D mode-I edge crack in an infinite domain is considered. Far field tensile stress $\sigma_0 = 10$MPa is applied in y-direction, and plane stress state is assumed. The Youngs modulus and the Poison's ratio of the plate is assumed to be 1GPa and 0.33, respectively. 3(c) shows the simulated circular domain; displacement boundary conditions along the circular boundary is set according the analytic solution. The set of polynomial bases used are given below. This setting is referred as 1^{st}-order PDS-FEM.

$$\begin{aligned} P^\alpha &= \{1, (x - x^\alpha), (y - y^\alpha)\} \\ Q^\beta &= \{1, (x - x^\beta), (y - y^\beta), (x - x^\beta)^2, (y - y^\beta)^2, (x - x^\beta)(y - y^\beta)\} \end{aligned}$$

Figure 7 shows σ_{yy} in the vicinity of the crack tip. It is found that except at a small neighbourhood of the crack tip, the stress component are accurate and the error diminishes at a second order rate. However, there is a significant error within the crack tip

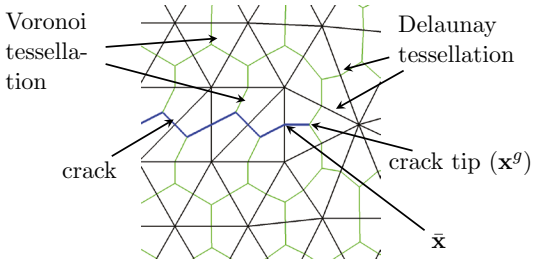

Figure 7: Change of mother point for the polynomial bases of crack tip element

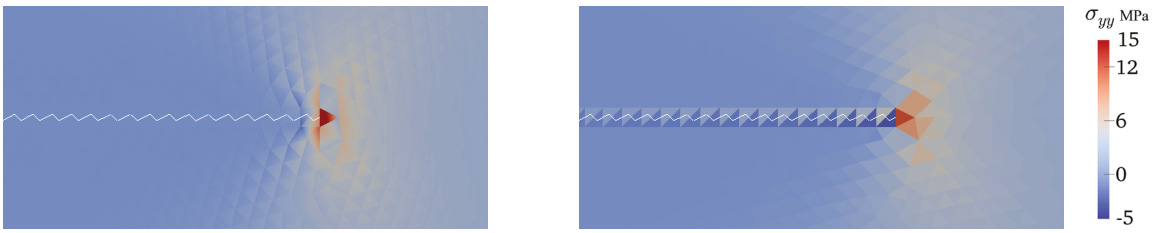

(a) 1^{st}-order PDS-FEM (b) 0^{th}-order PDS-FEM

Figure 8: σ_{yy} in the vicinity of the crack tip, with polynomial mother points moved to $\bar{\mathbf{x}}$.

element (i.e. element containing the crack tip). This deviation is not unexpected since crack tip singularity of $\sigma = f\left(\frac{1}{\sqrt{r}}, Sin\frac{\theta}{2}, Cos\frac{\theta}{2}\right)$ cannot be accurately approximated with polynomials. Judicious selection of bases function would be most appropriate approach to restore the stress singularity.

It is of interest to investigate the effect of the location of the mother point $\mathbf{x}^{\beta_c}$ of base polynomial set P^{β_c}, where Ψ^{β_c} is the Delaunay element containing the crack tip. As mentioned, mother points (i.e. center of area $\mathbf{x}^g$) of Ψ^β's are used as $\mathbf{x}^\beta$ in P^β. Polynomial bases with $\mathbf{x}^g$ may have negative effects in approximating singular stress field. To investigate the effect of setting $\mathbf{x}^\beta$ of the crack tip element to be outside of Ψ^{β_c}, a set of simulations are conducted with setting $\mathbf{x}^{\beta_c} = \bar{\mathbf{x}}$, where $\bar{\mathbf{x}}$ is the mid of broken edge as shown in Fig. 7(b).

Figure 8 shows σ_{yy} in the vicinity of crack tip with 0^{th}-order PDS-FEM and 1^{st}-order PDS-FEM. As is seen in Fig. 8(a) that choosing $\bar{\mathbf{x}}$ as polynomial mother point for Ψ^{β_c} rectifies the above problem in the crack tip element. Further, 1^{st}-order PDS-FEM has significant improvement in reproducing traction free condition along the crack surface, compared to 0^{th}-order. This is clearly visible in Fig. 9.

J-integral along a set of closed paths are evaluated for different sets of tessellation in order ot verify the crack tip stress singularity of 1^{st}-order PDS-FEM. According to Fig. 10 the error of J-integral diminishes at a rate of 1.4, while 0^{st}-order has first order rate [8].

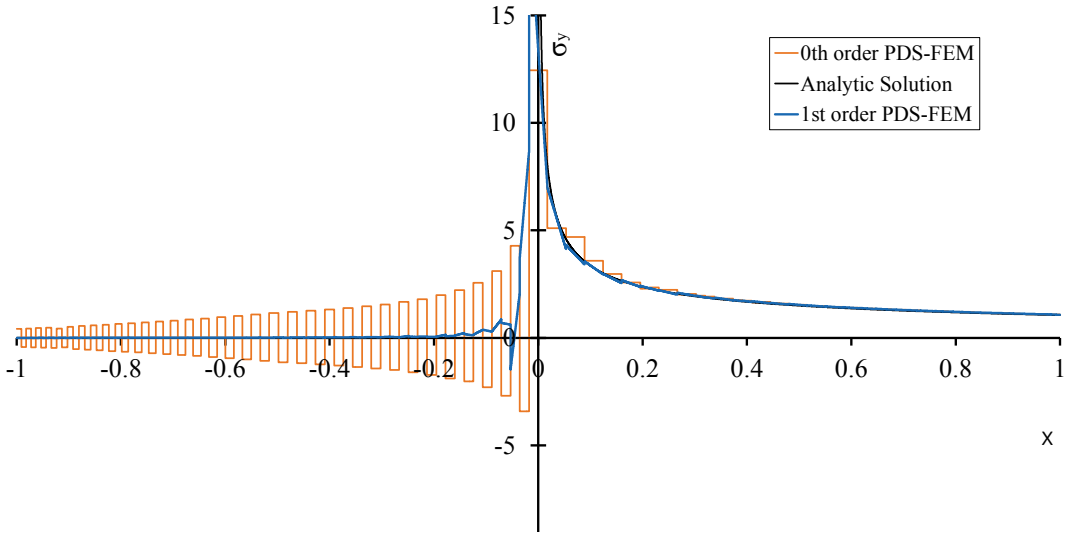

Figure 9: σ_{yy} along a section passing through the upper crack surface.

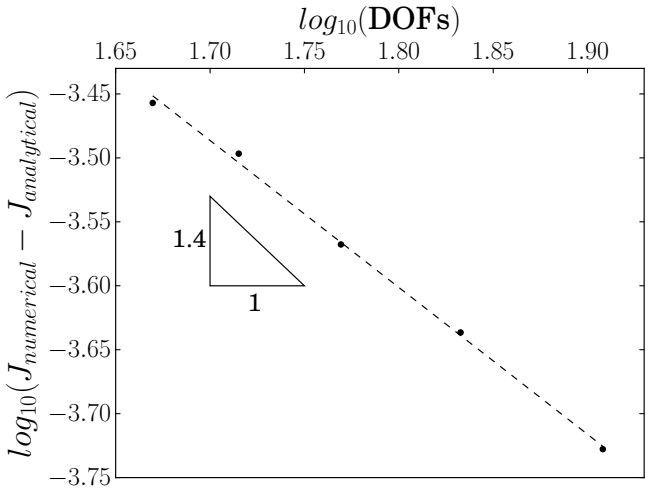

Figure 10: Convergence rate of J-Integral of mode-I edge crack problem with 1^{st}-order PDS-FEM.

5 CONCLUDING REMARKS

Higher order extension of PDS and PDS-FEM are presented. The verification tests indicates that second order convergence rate for displacement, strain and stress can be attained with first and second order polynomial sets for P^{α} and Q^{β}, respectively. While crack tip singularity also has higher accuracy, higher order PDS-FEM shows a significant improvement in reproducing traction free condition along the crack surface, compared to 0^{th}-order PDS-FEM.

REFERENCES

[1] S. Rahman, J.S. Kim,: Probabilistic fracture mechanics for nonlinear structures, Int. J. of Pressure Vessels and Piping, 78, pp. 261-269, 2001.

[2] Morsaleen Shehzad Chowdhury, Chongmin Song, Wei Gao,: Probabilistic fracture mechanics by using Monte Carlo simulation and the scaled boundary finite element method, Engineering fracture mechanics, 78, pp. 2369-2389, 2011.

[3] Benz W,: Smooth particle hydrodynamics: a review. In: Numerical Modeling of Nonlinear Stellar Pulsation: Problems and Prospects, Kluwer Academic, Boston, 1990.

[4] Belytschko T, Lu YY, and Gu L,: Element free galerkin methods. Int. J. Numer. Methods Eng. 37, pp. 229-256, 1994.

[5] Liu WK, Adee J, and Jun S,: Reproducing kernel and wavelets particle methods for elastic and plastic problems, In: Advanced Computational Methods for Material Modeling, AMD 180/PVP 268 ASME, pp. 175-190, 1993.

[6] Babuska I and Melenk JM,: The partition of unity method, Int. J. Numer. Methods Eng. 40, pp. 727-758, 1997 .

[7] Muneo Hori, Kenji Oguni, Hide Sakaguchi,: Proposal of FEM implemented with particle discretization scheme for analysis of failure phenomena, J. of Mech. and Phys. of Solids, Vol.53, pp. 681-703, 2005.

[8] M.L.L. Wijerathne, Kenji Oguni, Muneo Hori,: Numerical analysis of growing crack problem using particle discretization scheme, Int. J. for Numerical Methods in Engineering, Vol.80, pp. 46-73, 2009.

[9] Mahendra Kumar Pal, Lalith Wijerathne, Muneo Hori, Tsyushi Ichimura, Seizo Tanaka,: Implementation of Finite Element Method with higher order Particle Discretization Scheme, J. of Japan Society of Civil Engineers, Ser.A2 (Applied Mechanics(AM)),70(2), pp. 297-305, 2014.